THE ASTROPHYSICAL JOURNAL, 549:L203–L207, 2001 March 10

COLD H_2O AND CO ICE AND GAS TOWARD THE GALACTIC CENTER[1]

ANDREA MONETI,[2] JOSÉ CERNICHARO,[2,3] AND JUAN RAMÓN PARDO[3]

Received 2000 October 24; accepted 2000 December 7; published 2001 February 28

ABSTRACT

We present ice- and gas-phase observations of CO, ^{13}CO and of H_2O in the mid- and far-infrared taken with the *Infrared Space Observatory* (*ISO*) short- and long-wavelength spectrometers toward two positions in the Galactic center region (Sagittarius A* and GCS 3). These data are complemented with Caltech Submillimeter Observatory (CSO) observations of the $J = 3$–2 and $J = 7$–6 lines of CO. The *ISO* and CSO data indicate that the absorbing gas is extremely cold, $T_K \simeq 10$ K, suggesting that it is located in the dark clouds of the different spiral arms that intersect the lines of sight. From the analysis of the CO absorption, we derive ^{13}CO gas-phase column densities of 1.1 and 0.7×10^{17} cm^{-2} toward Sgr A* and GCS 3, respectively. The H_2O gas column density in the direction of Sgr A* is $\simeq 2 \times 10^{16}$ cm^{-2}. The derived CO/H_2O and gas/solid abundance ratios corresponding to these cold clouds are remarkably similar along the two lines of sight. We find that nearly all the CO is in the gas phase, while the H_2O is almost entirely frozen onto dust grains. Finally, the $N_{\rm gas+ice}({\rm CO})/N_{\rm gas+ice}({\rm H_2O})$ abundance ratio is $\simeq 5$, implying that H_2O formation processes are highly efficient.

Subject headings: infrared: ISM — ISM: abundances — ISM: individual (Sagittarius A*, GCS 3) — ISM: lines and bands — ISM: molecules

1. INTRODUCTION

The water molecule plays an important role in the chemistry of interstellar and circumstellar clouds, but due to its high abundance in the Earth's atmosphere, only some weak rotational lines (Cernicharo et al. 1990, 1994) are observable from the ground. It was only with the advent of the *Infrared Space Observatory* (*ISO*; Kessler et al. 1996) that extensive observations of the far-infrared thermal lines of water vapor could be used to obtain reliable estimates of the water vapor abundance in molecular clouds. Mapping of the Sagittarius B2 molecular cloud (Cernicharo et al. 1997b) has definitely shown that H_2O is a ubiquitous molecule in the cores of warm molecular clouds with an abundance of $\simeq 10^{-5}$. In addition, maps of the emission of several H_2O lines in Orion IRc2 have been obtained by Cernicharo et al. (1997a, 1999) showing that the abundance of H_2O is close to 10^{-4} in the shocked gas. H_2O observations of the central position of Orion have also been obtained by van Dishoeck et al. (1998), González-Alfonso et al. (1998), and Harwit et al. (1998). All these new data refer to the warm regions of molecular clouds. While there is also strong evidence for a high water depletion onto the ice mantles of dust grains in the coldest regions, no water vapor has been detected in the direction of dark clouds, probably because of the low temperature and density prevailing in these objects.

In order to study the coldest and least disturbed regions of molecular clouds, we have examined the *ISO* archive spectra of two positions in the Galactic center, where absorption from the intervening medium is known to occur (Lutz et al. 1996 and references therein). In the case of Sagittarius A*, this cold gas is also seen in the form of sharp and deep absorption features at 0, -30, and -50 km s^{-1} in various millimeter transitions of NH_3 and CO against the broad background produced by the warm clouds in Sgr A West (Serabyn & Güsten 1986; Sutton et al. 1990). The *ISO* data, together with submillimeter observations of the $J = 3$–2 and $J = 7$–6 lines of CO, have been modeled to place constraints on the abundances of these molecules in both the gas and the solid phases.

2. OBSERVATIONS

All data were obtained with the *ISO* short- and long-wavelength spectrometers (SWS: de Graauw 1996; LWS: Clegg et al. 1996) using the full-resolution grating mode of the SWS ($\lambda/\Delta\lambda \simeq 1500$–2000) and the grating and Fabry-Pérot (FP) modes of the LWS ($\lambda/\Delta\lambda \simeq 300$ and 9000, respectively). The effective SWS aperture in the 4–7 μm range is about $14'' \times 20''$, while the LWS aperture is circular and $\sim 70''$ in diameter. In both cases, the apertures include several sources (see Moneti et al. 2001 for GCS 3). The aperture centered on Sgr A* also includes several pointlike and diffuse sources. OLP 7.1 archive data were further processed with the ISAP package.[4] The results are shown in Figures 1, 2, and 3. In order to resolve the velocity structure of the absorbing/emitting gas in the direction of Sgr A*, we have made observations of the $J = 3$–2 and $J = 7$–6 lines of CO in the direction of this source with the Caltech Submillimeter Observatory (CSO). These observations were made in position switching, with the off position 4° outside the Galactic plane. A region of $10' \times 6'$ was mapped in the $J = 3$–2 line of CO, and a few positions were observed in the $J = 7$–6 line of the same species. The system temperatures at the frequencies of the $J = 3$–2 and $J = 7$–6 lines of CO were 760 and 6000 K, respectively, and the spectral resolution was 0.5 MHz. The results for the central position of our maps, Sgr A*, are shown in Figure 3.

3. RESULTS AND DISCUSSION

In order to determine the physical conditions of the foreground cold gas from the *ISO* H_2O and CO data, we have used

[1] Based on observations with the *Infrared Space Observatory*, an ESA project with instruments funded by ESA member states (especially the PI countries: France, Germany, the Netherlands, and the United Kingdom) and with the participation of ISAS and NASA.

[2] Consejo Superior de Investigaciones Científicas, IEM, Departament Física Molecular, Serrano 121, E-28006 Madrid, Spain; amoneti@astro.iem.csic.es, cerni@astro.iem.csic.es.

[3] Division of Physics, Mathematics, and Astronomy, California Institute of Technology, MS 320-47, Pasadena, CA 91125; pardo@submm.caltech.edu.

[4] ISAP is a joint development of the LWS and SWS instrument teams and data centers. Contributing institutes are CNRS, IAS, IPAC, MPE, RAL, and SRON.

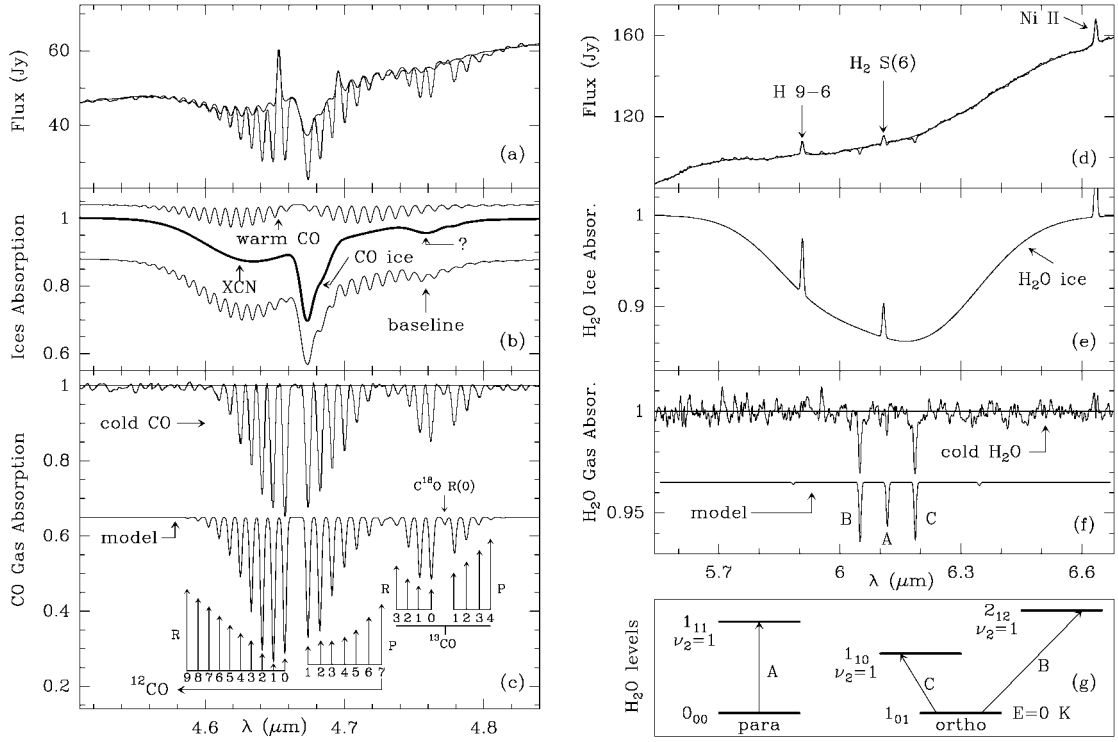

FIG. 1.—(*a–c*) *ISO* SWS spectra of the stretching mode of CO. (*d–f*) The bending mode of water vapor in the direction of Sgr A* (*ISO* observation number [ION] 46301102). Panels (*a*) and (*d*) show the observations and the continuum (including ices); (*b*) and (*e*) show the contribution of the ices and of the warm CO; (*c*) and (*f*) show the normalized spectrum and model spectrum (shifted for clarity); and (*g*) shows the details of the ortho- and para-H_2O transitions.

an LTE model with line parameters from the HITRAN molecular database (Rothman et al. 1993) to find the best fit to the line absorption. We note, however, that the energies of all ortho levels of H_2O are referred in HITRAN to the ground state of para-H_2O; i.e., the energy of the 1_{01} ground state of ortho-H_2O is not set equal to zero. For very low rotational temperatures, the derived physical parameters will have a large error if the HITRAN values of the energies and line intensities (which include a Boltzmann factor) are not corrected.

The $J = 7$–6 line of CO shows emission over a broad velocity range (see Fig. 3). The shape of this broad emission changes smoothly with position. This gas is certainly warm and emits in high-J lines of CO as shown in the LWS grating data of Sgr A* (see inset panel in Fig. 3*b*). The $J = 3$–2 line shows several narrow features in absorption against the broad component arising in the vicinity of Sgr A*. These narrow absorptions (see Fig. 3), at velocities of -5, -30, and -55 km s^{-1}, have also been seen in many other molecular and atomic species and correspond to cold gas in the line of sight that produces the series of R and P lines up to $J = 7$ in the rovibrational band of CO (see Fig. 1). The CSO maps indicate that the absorption features are present in all positions where the broad emission is seen. Hence, both broad emission and narrow absorption fill the *ISO* LWS and SWS beams. Consequently, prior to the analysis of the rovibrational absorption, the broad components due to the ices and, in the case of Sgr A*, to the warm CO gas in the Sgr A West region (Sutton et al. 1990), had to be analyzed and removed. In the following discussion, we will assume $X(\mathrm{CO}) = 10^{-4}$ and $^{12}\mathrm{CO}/^{13}\mathrm{CO} = 60$ (Langer & Penzias 1990).

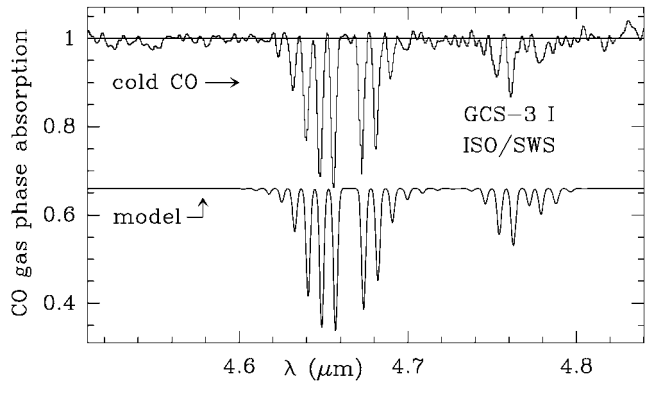

FIG. 2.—CO spectrum and model for GCS 3 (ION 32701543)

3.1. *Modeling the Warm* CO *Gas in Sgr A West*

The CO rovibrational data (SWS) have been modeled by a single component with $T_{\mathrm{rot}} = 150$ K, $\Delta v = 200$ km s^{-1}, and $N(\mathrm{CO}) = 1.0 \times 10^{17}$ cm^{-2}. The assumed line width is suggested by our $J = 7$–6 line data and by the LWS-FP observations of some CO lines (not shown here). The LWS grating data toward Sgr A* show CO pure rotational line emission from the $J = 14$–13 up to the $J = 21$–20 transitions (some of them are shown in the inset panel in Fig. 3*b*). Assuming that the emission fills the beam, and using a large velocity gradient code and the collisional rates of Schinke et al. (1985), the observed intensities are reproduced, within 20%–30%, for $n(\mathrm{H_2}) = 3 \times 10^5$ cm^{-3}, $T_K = 250$ K, $N(\mathrm{CO}) = 1.2 \times 10^{17}$ cm^{-2} with the assumed line width. The corresponding excitation temperatures vary between 160 and 180 K from the $J = 14$–13 to the $J = 21$–20 rotational lines of CO, i.e., similar to the rotation temperature derived from the SWS rovibrational absorption of CO. Note that the region is rather complex and that the column density we derive rep-

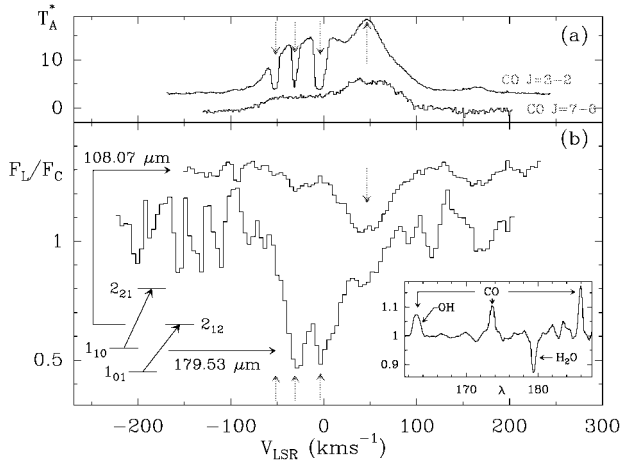

FIG. 3.—(*a*) $J = 3$–2 and $J = 7$–6 lines of CO toward Sgr A*. The downward arrows indicate the central position of the cold gas absorption features. The upward arrow indicates the velocity of the Sgr A* molecular cloud. (*b*) LWS-FP spectra of the 2_{12}–1_{01} and 2_{21}–1_{10} lines of ortho-H_2O toward Sgr A* (IONs 46300809 and 46900837). The drawing at bottom left indicates the transitions levels involved. The 1_{01}–2_{12} line shows three unresolved components at $v = -30$, -5, and 4 km s^{-1}, while in the other transition only the 4 km s^{-1} feature is present. The uncertainty in the absolute velocity is $\simeq$10–15 km s^{-1}. The inset panel shows the LWS grating spectrum (IONs 28701825, 32600211, 32702049, 49801004, 50501346, 67701010, 85302208, and 82800298); the CO and H_2O lines are indicated. The LWS-FP spectrum of ortho-H_2O has been shifted in velocity by one-third of the spectral resolution in order to match the velocity of the absorption features of other molecular species including CO. The upward arrows indicate the velocities of the cold absorbing gas, and the downward arrow that of the Sgr A* molecular cloud.

resents a beam-averaged value. Column densities for individual clouds could be larger and have to be derived using the corresponding filling factor and the correct line widths. The values for $n(H_2)$ and T_K are in excellent agreement with those derived by Sutton et al. (1990) for the individual warm clouds. The region of GCS 3 is free of molecular emission (Serabyn & Güsten 1991), and thus no such warm gas was used in the GCS 3 model.

3.2. *The* CO *and* H_2O *Ices*

The ices of CO, XCN, and H_2O are commonly found in the spectra of young, deeply embedded sources. The CO and XCN ice absorption bands were modeled as simple Gaussians; two Gaussians of different widths and central wavelengths were used for the polar and nonpolar CO ices (Chiar et al. 1998). The main goal of this fitting was to remove the CO ice contribution from the continuum; nevertheless, we could derive $N(\mathrm{CO\ ice}) \simeq 1.4 \times 10^{17}$ and $\simeq 0.7 \times 10^{17}$ cm^{-2} for Sgr A* and GCS 3, respectively, with ~70% apolar in Sgr A* and ~45% apolar in GCS 3. As for the H_2O ice, Chiar et al. (2000) used the same SWS data discussed here but considered both the 6 and 3 μm water ice features to determine $N(H_2O\ \mathrm{ice}) \simeq 1.2 \times 10^{18}$ and 5×10^{17} cm^{-2} for Sgr A* and GCS 3, respectively. The high fraction of apolar CO ice and the high $N(\mathrm{CO})/N(H_2O)$ ratios, together with the deep absorption of CO_2 ice (Whittet et al. 1997), are typical of cold, quiescent environments (Chiar et al. 1998), indicating that these ices cannot be located in the warm clouds in Sgr A West.

3.3. *The Cold* CO *Gas*

Because of the heavy saturation of the ^{12}CO rovibrational lines (opacities of about 20–30), the physical parameters of the cold CO gas were determined from the ^{13}CO and the adopted isotopic abundance ratio. Three components at the velocities indicated by the $J = 3$–2 absorption features in Figure 3 were used in the model, with line widths $\Delta v = 12$ km s^{-1} as measured in our data. These line widths agree well with the results shown in Figure 1 of Sutton et al. (1990). The derived model parameters (column density and rotation temperature) are the same for the three components. Model results can be found in Table 1. A single $C^{18}O$ velocity component was introduced in order to fit the weak $R(0)$ line of this isotope. We also find that in both lines of sight the cold gas alone is not sufficient to reproduce completely the ^{12}CO absorption, and a component of higher kinetic temperature, $T \simeq 40$ K, and $N \simeq 1\%$ of the total, is necessary to account for the highest observed J lines. This component cannot arise from an incomplete removal of the warm gas in Sgr A West, since it is present in both spectra, and should correspond to dense cloud material [$n(H_2) > 5 \times 10^4$ cm^{-3}] of low CO column density. We estimate uncertainties of about a factor of 2 in the column densities. The volume density needed to pump the observed rotational levels of the CO ground state is around 3×10^4 cm^{-3} in the case of $T_{\mathrm{rot}} \simeq 10$ K (Sgr A*), decreasing to $\simeq$1000 cm^{-3} at $\simeq$5 K (GCS 3). Adopting $A_V/N(H_2) \simeq 2 \times 10^{-21}$ mag cm^{-2}, the cold CO column densities imply visual extinction of 33 and 21 mag toward Sgr A* and GCS 3, respectively, generally consistent with values in the literature.

TABLE 1
MODEL RESULTS

Quantity	Sgr A*	GCS 3
Warm Gas		
T_K(CO and H_2O) (K)	250	...
T_{rot}(CO) (K)	$\simeq$150	...
$N(^{12}\mathrm{CO})$ ($\times 10^{17}$ cm^{-2})	1.0	...
$N(H_2O)$ ($\times 10^{15}$ cm^{-2})	1.0	...
Cold Gas		
T_{rot}(CO) (K)	6–12	5–10
$T_{\mathrm{rot}}(H_2O)$ (K)	8	...
$N(^{12}\mathrm{CO})$ ($\times 10^{18}$ cm^{-2})	6.6	4.2
$N(^{13}\mathrm{CO})$ ($\times 10^{17}$ cm^{-2})	1.1	0.7
$N(\mathrm{C}^{18}\mathrm{O})$ ($\times 10^{16}$ cm^{-2})	1.3	1.7
$N(H_2O)$ ($\times 10^{16}$ cm^{-2})	1.9	1.2

3.4. *The Cold/Warm* H_2O *Gas*

In contrast to CO, the H_2O absorption at 6 μm is weak: 3% (8 σ) in Sgr A* and 2% (3 σ) in GCS 3 (not shown). The three features detected are the 0_{00}–1_{11} (para) and the 1_{01}–1_{10} and 1_{01}–2_{12} (ortho) lines of the $\nu_2 = 0 \rightarrow 1$ vibrational transition of water vapor (see Fig. 1*f*). In the Sgr A* data, the para transition is blended with the H_2 (0, 0) $S(6)$ line, which was removed by assuming an intensity of one-third the average of the $S(5)$ and $S(7)$ lines. The para line of H_2O is present before the subtraction of the $S(6)$ line of H_2; however, its intensity is poorly determined. All three absorption features arise from the ground para and ortho states to the first excited rotational levels of the bending mode of water vapor. The lack of other H_2O absorption features indicates that all the water molecules are in the ground state (ortho and para). An ortho/para abundance ratio of 3 has been assumed.

The best fit to the H_2O absorption, assuming also the three velocity components of CO, is obtained for $T_{\mathrm{rot}} \simeq 8$ K, similar to the temperatures deduced from CO. While these H_2O lines are not very sensitive to temperature in the 3–12 K range, an upper limit of $T_{\mathrm{rot}} \lesssim 12$ K is obtained from the lack of ab-

sorption from the 1_{10} ortho level, which is 26.7 K above the ortho ground state (absorption from other levels of para-water is more difficult as the first excited level, the 1_{11}, is 53.4 K above the para ground state). The rovibrational line opacities are $\simeq 1$ and $\simeq 0.3$ for the ortho and para species, respectively. The column density of H_2O is 2×10^{16} cm^{-2}, with little dependence on the assumed Δv. This is due to the fact that line opacity and spectral dilution effects have inverse dependency on Δv for optically thin (τ below 1) lines.

The fact that the rotation temperature is low does not mean that the kinetic temperature is also low. While in the case of CO the inferred densities are high enough to make $T_{\rm rot} \simeq T_{\rm kin}$, the same is not true for H_2O. In order to determine what fraction of the absorbing H_2O belongs to which temperature component, we used the LWS-FP spectrum of the 1_{01}–2_{12} pure rotational line of ortho-H_2O (in the $\nu_2 = 0$ level) toward Sgr A* (see Fig. 3*b*). It indicates that the absorption arises from three different unresolved velocity components at -30, -5, and 45 km s^{-1}. The 1_{10}–2_{21} line, on the other hand, shows significant absorption only at 45 km s^{-1}. This cloud is probably the one associated to Sgr A* itself, and as for Sgr B2 (Cernicharo et al. 1997b), the analysis of the water vapor data is much more difficult due to the role of dust emission/absorption in the excitation of this molecule. Taking into account the absolute velocity accuracy of the LWS-FP, the -30 and -5 km s^{-1} features could correspond to the cold NH_3 (Serabyn & Güsten 1986) and CO $J = 3$–2 (see Fig. 3*a*). The CO absorption at -55 km s^{-1} is marginal in the LWS-FP data of H_2O. For the physical conditions of the cold gas, a minimum opacity of $\simeq 2$ with $\Delta v = 12$ km s^{-1} is needed to produce the observed absorption. It corresponds to $N(H_2O) > 2 \times 10^{14}$ cm^{-2}. However, with this column density the contribution of the cold H_2O to the rovibrational absorption (SWS) will be negligible. Can we derive more precisely this column density? An answer can come from the different opacities of the pure rotational and rovibrational lines of H_2O.

The line profiles of the water transitions differ remarkably from those of the CO lines observed with the CSO (see Fig. 3*a*) and with the LWS-FP (not shown). The warm gas in Sgr A West could also produce a broad H_2O absorption, and such absorption would appear as a baseline effect in the reduced velocity coverage of the LWS-FP spectra. Such a baseline has been removed from our data, but it is not possible to infer the possible contribution of the warm gas from these data. The grating data (see inset panel in Fig. 3*b*), however, show an absorption feature 13% deep at the wavelength of the 1_{01}–2_{12} line (and very weak absorption is also found for the 1_{10}–2_{21} line), which would require 4 times the absorption produced by the narrow lines of Figure 3*b*. Therefore, most of the absorption found in the grating spectrum must correspond to a broad velocity component badly detected with the LWS-FP. This broad absorption is also found in the 20 positions observed with the LWS grating spectrometer around Sgr A*.

The grating data suggest a line opacity of $\simeq 1$ for a line width of 200 km s^{-1}. From the physical conditions we have derived for the warm gas, the 1_{01}–2_{12} line opacity will be ~ 1 if $N(H_2O) = 10^{15}$ cm^{-2}. Hence, the H_2O abundance in the warm gas is 10^{-6}, similar to that found in the warm foreground gas of Sgr B2 (Cernicharo et al. 1997b; Neufeld et al. 2000). However, this column density that explains well the absorption excess in the LWS grating data is insufficient to explain the SWS absorption. Hence, we have to assume that the cold gas must have a larger column density to account for the SWS data.

Removing the contribution from the warm gas, the total column density of cold H_2O must be 1.9×10^{16} cm^{-2} (three velocity components). The opacity and excitation temperature of the 1_{01}–2_{12} rotational line will be $\simeq 90$ and 7 K, respectively, for each one of the three velocity components assumed. For GCS 3 we obtain a cold H_2O column density of $\simeq 1.2 \times 10^{16}$ cm^{-2}. These results suggest that the lines of sight intersect dense dark clouds where most of the absorption is produced. The $^{13}CO/H_2O$ abundance ratio would be $\simeq 5.8$ in both cases, i.e., $^{12}CO/H_2O \simeq 350$. Hence, $X(H_2O) \simeq 3 \times 10^{-7}$ and the water vapor gas/solid ratio is ~ 0.02 in the quiescent regions of dark clouds along the line of sight to the Galactic center.

The water vapor abundance in the dark clouds intersecting the line of sight of Sgr A* is much lower than that in the core of Sgr B2 and the shocked regions of Orion (see § 1). However, the total gas + ice CO/H_2O abundance ratio is $\simeq 5$, which means that a large fraction of the H_2O molecules in these cold, quiescent regions is condensed on grains and that the chemical mechanisms leading to its formation (either in gas phase or in the grain surface) are very efficient and make H_2O the most abundant molecular species after CO.

The *ISO* data corresponding to the pure rotational lines of H_2O toward Sgr A* alone provide a lower limit for the water abundance of $\sim 10^{-8}$. However, when combining these data with the rovibrational H_2O lines also observed by *ISO*, a larger abundance, $\simeq 10^{-7}$, is found. With this abundance, the pure 2_{12}–1_{01} and 1_{10}–1_{01} rotational lines of H_2O in the ground vibrational state will be extremely optically thick (see above), but the expected emission from these lines will remain very low. The upper limit to the water abundance derived through emission measurements by the *Submillimeter Wave Astronomy Satellite* (*SWAS*) in the direction of TMC-1 (7×10^{-8}; Snell et al. 2000) is only of factor of 4 lower than the value we derive in the dark clouds toward Sgr A*. If we consider that in dark clouds important scattering effects have to be taken into account in the radiative transfer of optically thick lines (see Cernicharo & Guélin 1987), the upper limit derived by *SWAS* could be slightly underestimated. Therefore, our results for Galactic dark clouds toward Sgr A* and *SWAS* results for TMC-1 would be in a relatively good agreement. Finally, absorption measurements toward continuum background sources at 556.9 GHz (1_{01}–1_{10}) and at 179.526 and 269.273 μm (1_{01}–2_{12} and 0_{00}–1_{11}) with future satellite missions such as *FIRST* will provide a very efficient way to derive the water vapor abundance in dark clouds and in the diffuse interstellar medium.

We thank Spanish DGES for this research under grants PB96-0883 and ESP98-1351E. We thank E. González-Alfonso for useful comments. The CSO is supported by NSF grant AST 99-80846.

REFERENCES

Cernicharo, J., González-Alfonso, E., Alcolea, J., Bachiller, R., & John, D. 1994, ApJ, 432, L59

Cernicharo, J., González-Alfonso, E., & Lefloch, B. 1997a, in First *ISO* Workshop on Analytical Spectroscopy, ed. A. M. Heras, K. Leech, N. R. Trams, & M. Perry (ESA SP-419; Noordwijk: ESA), 23

Cernicharo, J., & Guélin, M. 1987, A&A, 176, 299

Cernicharo, J., Thum, C., Hein, H., John, D., Garcia, P., & Mattioco, F. 1990, A&A, 231, L15

Cernicharo, J., et al. 1997b, A&A, 323, L25

Cernicharo, J., et al. 1999, in The Universe as Seen by *ISO*, ed. P. Cox & M. F. Kessler (ESA SP-427; Noordwijk: ESA), 565
Chiar, J. E., Geriakines, P. A., Whittet, D. C. B., Pendelton, Y. J., Tielens, A. G. G. M., Adamson, A. J., & Boogert, A. C. A. 1998, ApJ, 498, 716
Chiar, J. E., Tielens, A. G. G. M., Whittet, D. C. B., Shutte, W. A., Boogert, A. C. A., Lutz, D., van Dishoeck, E. F., & Bernstein, M. P. 2000, ApJ, 537, 749
Clegg, P. E., et al. 1996, A&A, 315, L38
de Graauw, Th., et al. 1996, A&A, 315, L49
González-Alfonso, E., Cernicharo, J., van Dishoeck, E. F., Wright, C. M., & Heras, A. 1998, ApJ, 502, L169
Harwit, M., Neufeld, D. A., Melnick, G. J., & Kaufman, M. J. 1998, ApJ, 497, L105
Kessler, M. F., et al. 1996, A&A, 315, L27
Langer, W. D., & Penzias, A. A. 1990, ApJ, 357, 477
Lutz, D., et al. 1996, A&A, 315, L269
McFadzean, A. D., Whittet, D. C. B., Longmore, A. J., Bode, M. F., & Adamson, A. J. 1989, MNRAS, 241, 873
Moneti, A., Stolovy, S. R., Blommaert, J. A. D. L., Figer, D. F., & Najarro, F. 2001, A&A, 366, 106
Neufeld, D. A., et al. 2000, ApJ, 539, L111
Rothman, L. S., et al. 1993, J. Quant. Spectrosc. Radiat. Transfer, 48, 469
Schinke, R., Engel, V., Buck, U., Meyer, H., & Diercksen, G. H. F. 1985, ApJ, 299, 939
Serabyn, E., & Güsten, R. 1986, A&A, 161, 334
———. 1991, A&A, 242, 376
Snell, R. L., et al. 2000, ApJ, 539, L101
Sutton, E. C., Danchi, W. C., Jaminet, P. A., & Masson, C. R. 1990, ApJ, 348, 503
van Dishoeck, E. F., Wright, C. M., Cernicharo, J., González-Alfonso, E., de Graauw, Th., Helmich, F. P., & Vandenbussche, B. 1998, ApJ, 502, L173
Whittet, D. C. B., et al. 1997, ApJ, 490, 729